Hindawi
International Journal of Photoenergy
Volume 2019, Article ID 1609234, 17 pages
https://doi.org/10.1155/2019/1609234

Research Article

Numerical Investigations on Charging/Discharging Performance of a Novel Truncated Cone Thermal Energy Storage Tank on a Concentrated Solar Power System

Qianjun Mao,[1] **Ning Liu**,[1] **and Li Peng**[1,2]

[1]*School of Urban Construction, Wuhan University of Science and Technology, Wuhan 430065, China*
[2]*College of Chemistry and Chemical Engineering, Northeast Petroleum University, Daqing 163318, China*

Correspondence should be addressed to Qianjun Mao; maoqianjun@163.com and Li Peng; sjkpl@163.com

Received 9 August 2018; Revised 10 October 2018; Accepted 30 October 2018; Published 27 January 2019

Guest Editor: Mattia De Rosa

Developing a concentrated solar power (CSP) technology is one of the most effective methods to solve energy shortage and environmental pollution all over the world. Thermal energy storage (TES) system coupling with phase change materials (PCM) is one of the most significant methods to mitigate the intermittence of solar energy. In this paper, firstly, a 2D physical and mathematical model of a novel truncated cone shell-and-tube TES tank has been proposed based on enthalpy method. Secondly, the performance during the charging/discharging process of the truncated cone tank has been compared with the traditional cylindrical tank. Finally, the effects of inlet conditions of heat transfer fluid (HTF), and thickness of tube on the charging/discharging process, stored/released energy capacity; energy storage/release rate and heat storage efficiency have been investigated. The results show that the performance of truncated cone tank is better, and the charging/discharging time reduces 32.08% and 21.59%, respectively, compared with the cylindrical tank. The effect of wall thickness on the truncated cone TES tank can be ignored. And the inlet temperature and velocity of HTF have the significant influence on the charging/discharging performance of TES tank. And the maximum heat storage efficiency of the truncated cone TES tank can reach 93%. However, some appropriate methods should be taken for improving the thermal energy utilization rate of HTF in the future. This research will provide insights and significant reference towards geometric design and operating conditions in TES system.

1. Introduction

The sustainable development of low-carbon economy has become the inevitable choice to realize the win-win situation of economic development and environmental protection around the world. To alleviate the associated environmental problems, reduction of the use of fossil fuels by developing more cost-effective renewable energy technologies becomes increasingly significant. Among various types of renewable energy sources, solar energy takes a large proportion [1–3]. And many believe that actively developing CSP technology is one of the most effective ways to solve current global energy supply problems. However, one major drawback of solar energy is intermittence. To mitigate this issue, the need for energy storage system arises in most of the areas where CSP technology is utilized [4, 5].

The thermal energy can be stored in different forms, such as sensible heat, latent heat, thermochemical, or a combination of these [6]. In sensible thermal storage, the thermal energy is temporarily stored with rise/fall temperature in the storage media. In latent thermal storage, the considerable latent heat of PCM is absorbed/desorbed in the phase transition process for storing/releasing thermal energy, and this system with PCM owns the advantages of nearly constant temperature and much higher energy density per unit volume compared to the sensible thermal storage. And in thermochemical thermal storage, large amount of enthalpy change in endothermic/exothermic chemical reactions is used to store/release thermal energy,

and the approach is still in the laboratory research stage due to its complexity, safety, and harsh operation condition [7–9]. Thus, latent thermal storage system with PCM is now an effective and feasible solution to store thermal energy in CSP plants.

Avci, Dadollahi, Tao et al. [10–12] investigated the effect of the inlet condition of HTF on the thermal energy storage performance of a cylindrical shell-and-tube TES system for CSP technology. The results indicated that the increase of inlet temperature and velocity of the HTF can enhance the charging performance and energy storage capacity in a TES system. Fang et al. [13] proposed an index of effective energy storage ratio to characterize the effective energy storage capacity of LHTES system with the same volume of tube-in-tank design. The analysis provided implications on an optimal design of LHTES systems in practical CSP plants. Assari et al. [14] studied the TES performance with the different inlet and outlet location of the fluid in horizontal cylindrical tank by numerical and experimental method. The results showed that an appropriate location for the hot water inlet resulted in better thermal stratification in the storage tank, in addition, an appropriate location for the cold water outlet resulted a better collector efficiency, which both increased the performance of solar water heater system.

Many researchers found that the natural convection had a great influence on the charging process in TES system. Seddegh et al. [15] studied the influence of natural convection on charging/discharging of vertical cylindrical TES tank, which was developed to experimentally investigate how the natural convection is initiated and how the energy is transferred from the HTF to PCM in the LHTES system. Tao and He [16] investigated the influence of natural convection and the fins on performance of horizontal latent heat storage tank. The results showed that the high temperature molten salt flows upward which enhances the PCM melting rate in upside and weakens the melting rate in downside due to the effects of natural convection. Kurnia and Sasmitob [17] proposed a rotating TES system to overcome the shortcoming of natural convection. The results revealed that rotation does increase the heat transfer performance, and this system with up to 25% and 41% enhancement can be achieved during charging and discharging, respectively. Gao et al. [18] investigated the thermal performance of the cubic TES system with coil tubes. The results showed that natural convection accelerated the thermal energy transport in the melt phase in the upper region but weakened the heat transfer in the bottom region.

In general, the molten salt is one of the most promising PCM used in CSP plant; however, the main shortcomings of them are low thermal conductivity, and a lot of works have been studied to overcome this issue and to enhance the heat transfer rate of TES tank in CSP system. Parsazadeh, Yang et al. [19, 20] investigated the melting process in shell-and-tube TES system with annular fins. The numerical results showed that the fins exhibited a promising potential for enhancing heat transfer in CSP technology. Amagour et al. [21] studied the finned-tube LHTES system based on the method of equivalent circular fin efficiency for the calculation of the effective heat transfer surface area. And the compact finned-tube system presented a satisfactory overall performance compared to other published results. Gasia et al. [22] compared the performance of TES in four systems including the addition of fins and the use of two different HTF. The results revealed that the finned designs showed an improvement of up to 40% for the same HTF, and water showed results up to 44% higher than silicone for the same design. Zhu, Eslami et al. [23, 24] studied the transient behavior of the rectangular thermal energy tank equipped with fin configurations. The results showed that the fins can obviously enhance the thermal performance. Parsazadeh and Duan [25] analyzed the influence of nanoparticles added on HTF and PCM on a shell-and-tube TES system for CSP technology.

In addition, the packed bed LHTES system with spherical capsules has been studied in recent years for enhancing the heat transfer rate in CSP plants. Bellan et al. [26] analyzed the dynamic thermal performance of high temperature latent thermal energy system packed with spherical capsules. The results indicated that the Stefan number and the shell properties of the capsule significantly influence the thermal performance of the system. Ma and Zhang [27] adopted Al-Si and air as the PCM and HTF, respectively, and built the packed bed system. The results showed that the performance of PCM is better than rock due to the high latent heat and thermal conductivity of the PCM (alloy). Abdulla and Reddy [28] investigated the thermal performance of a packed-bed thermocline TES system, and it was found that the relative to inlet salt velocity and operating temperature range have more influence on the thermal performance of TES system.

It is clear from the literature reviewed above that the natural convection accelerated the thermal energy transport in the upper region and weakened the heat transfer in the bottom region during the charging process [16, 18]. And the shell-and-tube TES system is the promising design to store energy due to its symmetrical structure and simple analysis. Therefore, this paper proposed a novel truncated cone shell-and-tube TES tank of CSP plant to enhance the heat transfer by taking advantage of natural convection. And it is compared with the performance of traditional cylindrical TES tank. A 2D model is built to numerically investigate the effects of inlet temperature, velocity of the HTF, and the thickness of tube on the charging/discharging performance with this novel TES system. This research will provide a significant reference towards geometric design and operating conditions by considering the effect of natural convection on a TES system for CSP plant.

2. Physical Model and Governing Equations

2.1. Physical Model of a Novel Truncated Cone Tank. The physical model is shown in Figure 1, which is a truncated cone shell-and-tube configuration. The HTF flows in the inner tube, and the shell side is full of PCM with the mass of 54% $NaNO_3$ and 46% KNO_3. The length (L) of this tank is 200 mm, the radius for the inner tube (R_{in}) is 20 mm, and the material of the inner tube is steel. In addition, the container external surface is treated as an adiabatic

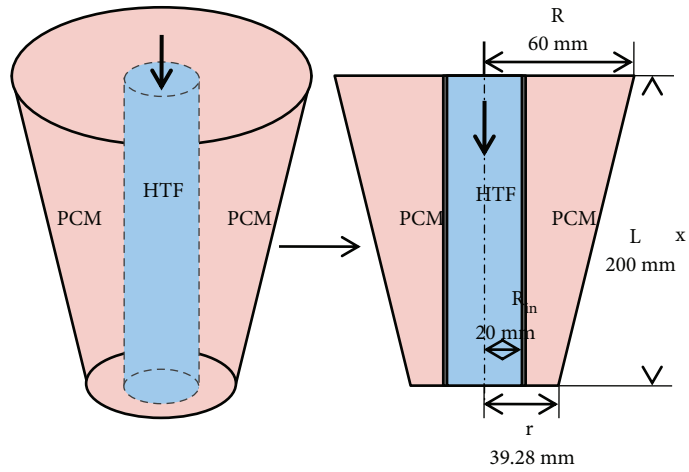

Figure 1: Schematic diagram of a truncated cone shell-and-tube TES model.

boundary with the radius of the top and bottom as 60 mm (R) and 39.28 mm (r), respectively, and the taper of this truncated cone model is 0.2072. Under the condition of the constant volume/mass of the PCM and the same radius of the inner tube, the traditional cylindrical shell-and-tube model is built and simulated. The thermophysical properties of PCM are shown in Table 1.

In order to simplify the physical and mathematical model, the following assumptions are adopted [8, 29].

(1) The HTF flow entering the tube was laminar and simultaneously developing

(2) The thermal conduction and viscous dissipation in the axial direction is neglected for PCM

(3) The thermal properties of PCM in both solid and liquid phase do not change with the temperature

(4) Adiabatic wall was assumed

(5) The models are simplified to 2D axisymmetric

2.2. Governing Equations. The enthalpy method is adopted to deal with the moving boundary problem in a solid-liquid phase change process. The corresponding governing equations are shown as follows [12, 30].

For the HTF,

$$\frac{\partial \theta_f}{\partial t} = -A\frac{\partial \theta_f}{\partial x} - B\left(\theta_f - T\right)_a, \tag{1}$$

where $\theta_f = T - T_m$; $A = \dot{m}_f/\rho_f \pi R_{in}^2$, $B = 2h/(\rho C_p)_f R_{in}$. $h = (k/2R_{in})0.022P_r^2 R_e^{0.8}$, and T_a is the average temperature of the PCM and T_m is the melting temperature.

For the PCM,

$$\left(\rho C_p\right)_p \frac{\partial \theta}{\partial t} = \frac{\partial}{\partial x}\left(\lambda_p' \frac{\partial \theta}{\partial x}\right) + \frac{1}{r}\frac{\partial}{\partial r}\left(r\lambda_p \frac{\partial \theta}{\partial r}\right) - \rho_p \Delta H \frac{\partial f}{\partial t}, \tag{2}$$

where $\theta = T - T_m$, f is the liquid fraction of the PCM, ΔH is the PCM melting enthalpy. λ' and λ_p are the thermal conductivity of PCM in x and r direction (W/m·K).

Table 1: Thermophysical properties of PCM.

	PCM ($NaNO_3/KNO_3$)
ρ (kg/m^3)	2040(s), 1950(l)
λ (W/m·K)	0.5(s), 0.3(l)
C_p (J/kg·K)	1420(s), 1500(l)
T_m (K)	497
ΔH (kJ/kg)	105.8

*The "(s)" and "(l)" stand for "solid" and "liquid" of PCM, respectively.

The energy equation (2) is formulated by enthalpy method. And the liquid fraction is determined as

$$\begin{cases} f = 0, \theta < 0, \\ 0 < f < 1, \theta = 0, \\ f = 1, \theta > 0. \end{cases} \tag{3}$$

To calculate the stored energy of the PCM, the stored energy capacity of the TES system is given by [31]

$$Q = m\int_{T_0}^{T_m} C_{p,s}dT + mf\Delta H + m\int_{T_m}^{T_a} C_{p,l}dT. \tag{4}$$

Meanwhile, the released energy capacity of the TES system is given by

$$Q' = m\int_{T_0}^{T_m} C_{p,l}dT + mf\Delta H + m\int_{T_m}^{T_a} C_{p,s}dT, \tag{5}$$

where m is the mass of PCM (kg), T_0 is the initial temperature of the PCM (K), T_m is the melting temperature and T_a is the average temperature of PCM at the end of melting process (K), f is the liquid fraction of PCM, and ΔH is the enthalpy of fusion (kJ/kg). Meanwhile, $C_{p,s}$ and $C_{p,l}$ represent the specific heat of the PCM at the state of

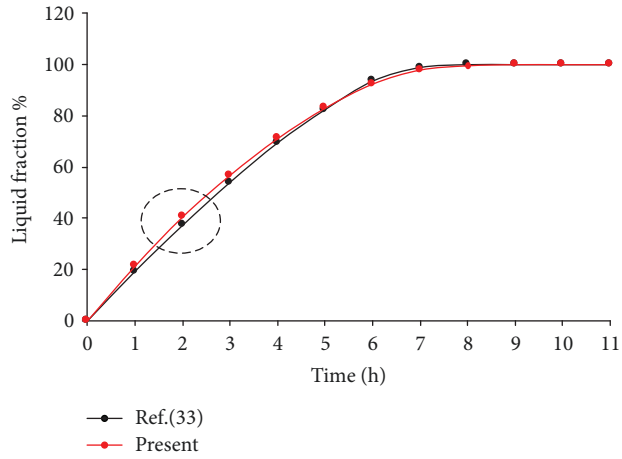

Figure 2: Comparison between the present result and the result of literature Ref. [32].

solid and liquid (kJ/kg·K), respectively. The equation has three parts with the first part representing sensible heat stored in the solid phase, the second part represents latent heat of fusion, and the third part represents sensible heat stored in PCM in the liquid phase.

3. Model Validation and Testing

The finite volume solver ANSYS Fluent 16.0 is used to discrete the governing equations. Due to the coupled energy transfer process between the HTF and PCM, the energy equation both for HTF and for PCM is integrated solving in the whole computational domain. Accordingly, to calculate the Reynolds number of HTF ($Re_{max} = 1654 < 2300$, $v_{max} = 1.2$ m/s), the laminar is selected as the flow model. And the coupled fluid dynamic and energy equations are solved by SIMPLEC algorithm. The second order upwind method is applied as the spatial discretization method for pressure, momentum, and energy. In order to ensure the accuracy of the calculation, the residual of the energy equation is less than 10^{-6}.

In order to validate the reliability of the physical model, the setting, calculation, and simulation results based on Fluent 16.0 software, the comparisons between the present numerical predictions, and the literature results which is the theoretical analysis by C language in MATLAB software [32] were performed under the same geometric parameters and operation conditions. The comparative results are shown in Figure 2. In the plots, the melting time is approximately 7 h both of the two methods, and the melting time error is about 6.67%. Meanwhile, the maximum melting error is about 8.70% at 2 h, which is shown in the dashed circle. The results show that these errors (8.7% and 6.67%) are within the allowable range of engineering errors. Therefore, the good agreements show that the physical model and simulation results based on Fluent 16.0 software in the present paper are acceptable and reliable. It can be seen that the settings of Fluent 16.0 here can be used for simulation experiments.

Table 2: The results of mesh independent and time step independent test.

Total mesh	Total melting time (s)	Time step (s)	Total melting time (s)
12,400	6926	0.05	6939
24,080	6936	0.1	6941
46,224	6942	0.5	6942
92,017	6953	1	6953
179,177	6961	2	6979

The mesh of this model consists of the quadrilateral cells. To ensure mesh independent result, mesh independence test was conducted by systematically increasing the number of cell and the results as shown in Table 2. The results did not show a significant change in the total melting time as the number of cells increases to 179,177. Therefore, in order to save the computational time, the mesh size of 46,224 cells for the truncated cone shell-and-tube TES model was chosen for the simulations. Besides, the maximum and minimum time steps are 2 s and 0.05 s, respectively. And the Courant number is the default value. Accordingly, to analyze the total melting time of the five cases, the time step size of 0.5 s was the most appropriate to be accounted for the transient nature of the model and the results as shown in Table 2.

4. Results and Discussions

4.1. The Charging Process of TES

4.1.1. Comparison of the TES Performance between Cylindrical and Truncated Cone TES Model in Charging Process. In order to compare the TES performance between traditional cylindrical and truncated cone TES tanks, the inlet temperature and velocity of HTF are 797 K and 1.2 m/s, respectively.

The contour of the PCM liquid fraction and temperature flied in the cylindrical and truncated cone tank during the melting process are shown in Figure 3. It is noted that the melting starts on the tube wall surface and expands inside the PCM, and the upper region of the PCM is melting first compared to the lower region. From the corresponding temperature field, it can be found that the temperature shows an obvious ladder distribution, and the temperature closing to the heat pipe region and the top region of the PCM is higher. This phenomenon can be explained in terms of heat conduction and natural convection. On the one hand, the temperature difference is larger in the upper region of the PCM and HTF, so that the heat transfer rate is faster in this region. On the other hand, the higher-temperature liquid PCM rises because of the effect of natural convection, which promotes the melting of the upper PCM. However, the influence of the heat conduction can be ignored in the heat transfer process, because the length of these two models studied in this paper is identical.

According to the melting time and liquid fraction in Figure 3, on the whole, the truncated cone tank can melt

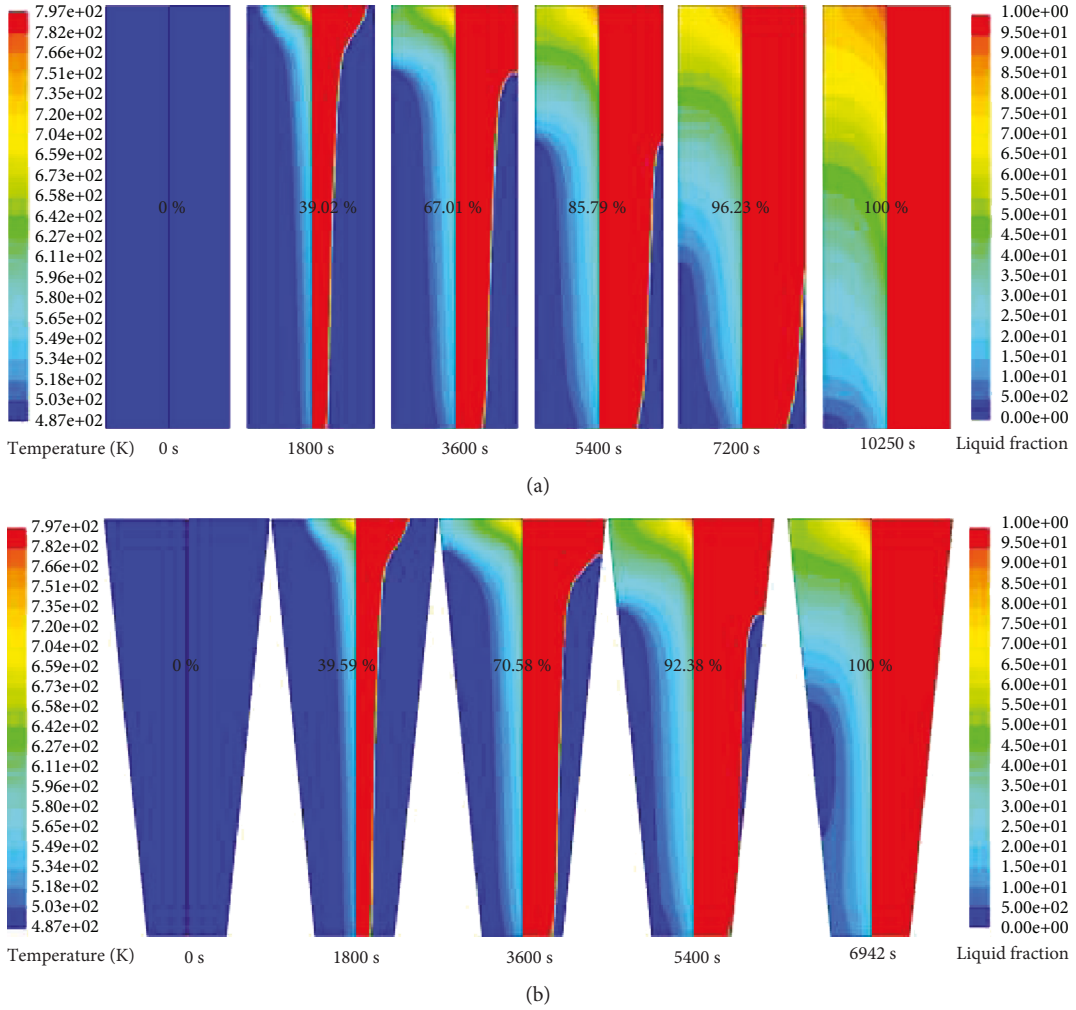

Figure 3: Contour of the PCM temperature (left) and liquid fraction (right) in the (a) cylindrical and (b) truncated cone model during the charging process.

much faster than the cylindrical tank at the same operating condition during the process. However, the liquid fraction of a truncated cone tank is about 40%, which is equal to the liquid fraction of a cylindrical tank at 1800 s. After that, the melting process of a truncated cone tank is obviously quicker than a cylindrical tank, and the total melting time reduces about 32.08% compared with the cylindrical tank. This indicates that the thermal energy storage performance of a truncated cone tank is better and the melting process is faster than the cylindrical tank under the same operating condition.

Figure 4 presents the simulated liquid PCM velocity field with a cylindrical and truncated cone TES tank during the melting process, which can explain the reason of the upper region of PCM melt faster than the lower region of PCM. It can be seen that the clockwise convection circulation arises at the liquid region of PCM, and the high-temperature liquid PCM at the vicinity of the HTF pipe flows upward due to the effect of natural convection, whereas the low-temperature liquid PCM flows downward along the liquid/solid interface of PCM because of the action of natural gravity. In this situation, the natural convection accelerates the thermal energy transfer at the top region and weakened the thermal energy transfer at the bottom region of the PCM. Therefore, the truncated cone tank can obviously reduce the melting time compared to the cylindrical TES tank.

4.1.2. Effects of Thickness of Tube on Charging Process. In order to study the effect of thickness of tube on the TES performance during the charging process, the inlet temperature and velocity of HTF are 797 K and 1.2 m/s, respectively, and the initial temperature of PCM and tube is 487 K. Meanwhile, the radius for the inner tube (R_{in}) is always 20 mm.

Figure 5 presents the effects of different thickness of tube on liquid fraction and melting process. It can be seen that the liquid fraction of PCM decreases with the increasing thickness of tube in the early stage. The possible reason is that the thermal resistance increases with the increase of the thickness of the tube lead to the melting rate reduce. And after that, the liquid fraction increases with the increasing thickness of tube during the melting process. That is because the increasing thickness of the tube makes the mass

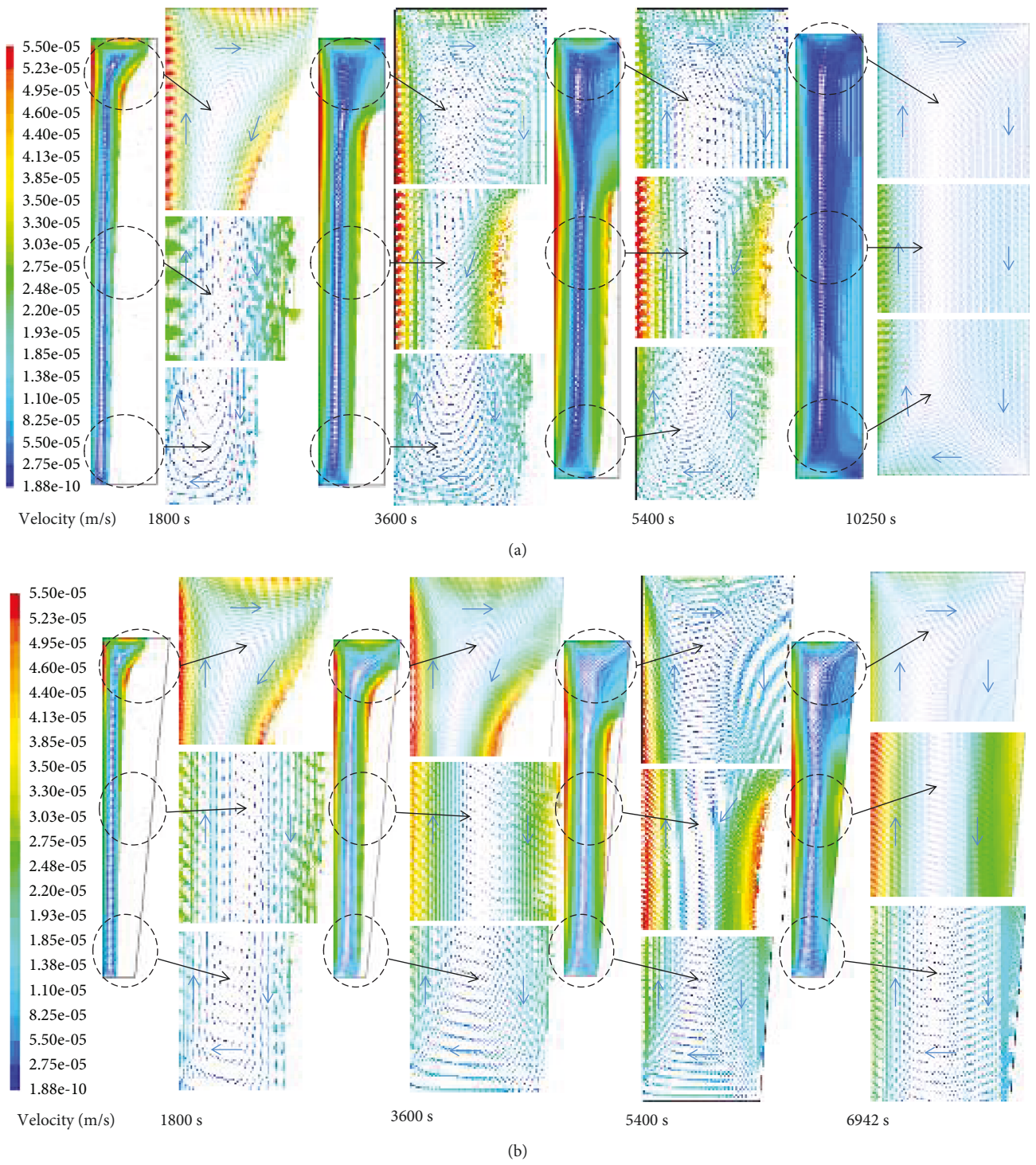

Figure 4: The simulated liquid PCM velocity field with cylindrical (a) and truncated cone (b) TES unit during the melting process.

of PCM reduce slightly, as a whole, the melting time of PCM will be slightly reduced with the decrease of the PCM. And the influence of the thickness of tube on the melting time gradually weakens with the increasing of the wall thickness. However, the reduction of the melting time can be negligible compared to the case where the wall thickness is neglected. Therefore, the effect of wall thickness on the truncated cone TES system is ignored in the rest of the studies.

4.1.3. Effects of Inlet Temperature of HTF on Charging Process. The initial temperature of PCM with 487 K, and the inlet velocity of HTF with 1.2 m/s is chose to study the effects of inlet temperature of HTF on the melting process. And the inlet temperature of the HTF is six temperature gradients, including 597 K, 647 K, 697 K, 747 k, 797 K, and 847 K.

The effects of inlet temperature of HTF on melting process are shown in Figure 6, which include the charging

process of a cylindrical TES tank under the inlet temperature of HTF at 797 K. It can be seen that the melting time decreases with the increasing inlet temperature of HTF, and the slope of this curve is larger in the early stage. Higher temperature difference between HTF and PCM leads to the heat transfer rate increasing. At the same time, it can be seen that the higher the inlet temperature of the HTF is, the bigger the slope of the melting curve is and the higher the heat storage rate of the PCM is. And under the same operating conditions (the inlet temperature of HTF is 797 K), the charging time of the truncated cone TES tank is shorter than that of the cylindrical tank. The results are consistent with the contour of the PCM liquid fraction and temperature in the cylindrical and truncated cone tank during the charging process.

The effects of initial inlet temperature of HTF on the outlet temperature of HTF are presented in Figure 7. Meanwhile, the numbers represent the total melting time during the charging process. From Figure 7, the initial inlet temperature increasing from 597 K to 847 K, the melting time will decrease from 15,111 s to 6262 s, which reduces about 58.56%. And the outlet temperature increases with the increasing initial inlet temperature. For each case, the outlet temperature of the HTF increases slowly during this process. As a whole, the higher the inlet temperature of the HTF, the greater the temperature difference between the inlet and the outlet temperature. And when the inlet temperature is 847 K, the corresponding minimum outlet temperature is 786 K, and the temperature difference is about 60 K. It can be seen that the thermal energy utilization rate from HTF is very low during this process. Therefore, some methods should be taken to reduce the loss of energy and improve the thermal energy utilization rate of HTF in the TES system for enhancing the CSP plant efficiency.

Figure 8 presents the effects of initial inlet temperature of HTF on the total stored energy capacity and energy storage rate during the charging process. The histogram and curve show the total stored energy capacity and total energy storage rate of the TES tank, respectively. And the value of the total stored energy capacity is calculated by equation (4). The total energy storage rate is calculated by following equation.

$$v_Q = \frac{Q}{t}, \tag{6}$$

where the v_Q represents the total energy storage rate (J/s), Q is the total stored energy capacity (J), and t is the charging time (s).

The histogram indicates that the total stored energy capacity and initial inlet temperature of HTF has notable positive correlation, and the initial inlet temperature of HTF increasing from 597 K to 847 K, the total stored energy capacity will increase from 506.55 kJ to 753.21 kJ, which increases about 48.69%. However, the increment of stored energy capacity decreases with the increase of inlet temperature. Meanwhile, the curve shows that the total energy storage rate increases significantly with the increase of inlet temperature, and the inlet temperature increasing from 597 K to 847 K, the energy storage rate will increase from 33.52 J/s to 120.28 J/s, which increases about four times.

It is shown that the inlet temperature of HTF has the significant influence on the TES system for a truncated cone shell-and-tube tank. The increase of inlet temperature can not only shorten the total charging time but also increase the total stored energy capacity and energy storage rate. Therefore, it is very important to select the proper inlet temperature of HTF according to the actual operating conditions to improve the storage efficiency of the TES system in the CSP plant.

4.1.4. Effects of Inlet Velocity of HTF on Charging Process. In order to study the effect of the inlet velocity of HTF on the charging process of the TES tank, the initial temperature of the PCM and HTF is 487 K and 797 K, respectively. And the inlet velocity of the HTF is six temperature gradients, including 0.2 m/s, 0.4 m/s, 0.6 m/s, 0.8 m/s, 1.0 m/s, and 1.2 m/s.

Figure 9 presents the effects of inlet velocity of HTF on liquid fraction during the charging process. As a whole, the slope of the melting curve decreases gradually in the charging process of liquid fraction up to 100%. And the charging time decreases with the increasing inlet velocity of HTF, because the higher velocity of HTF makes the temperature difference between HTF and PCM augment, which leads to the heat transfer rate increasing. With the increase of inlet velocity, the effect of HTF on charging time becomes smaller and smaller.

The effect of inlet velocity on outlet temperature of HTF is presented in Figure 10. The result shows that the outlet temperature increases with the increase of the inlet velocity of HTF. From the curves, the tendency of outlet temperature is rather gradual during the process. However, the outlet temperature difference of HTF is decreasing with the increasing initial inlet velocity. It was found that increasing the velocity of HTF from 0.2 m/s to 1.2 m/s reduces the melting time from 11,334 s to 6972 s by 38.48%. And when the inlet velocity of HTF is 0.2 m/s, the outlet temperature is the smallest (the minimum outlet temperature of 695 K), and the maximum temperature difference is 102 K. At this time, there is still a large amount of heat energy to not be utilized from the HTF.

Figure 11 presents the effects of inlet velocity of HTF on the total stored energy capacity and total energy storage rate during the process. The histogram shows that the total stored energy capacity of the TES tank increases with the increase of the inlet velocity of HTF, but the increasing amplitude is decreasing gradually. And the inlet velocity increasing from 0.2 m/s to 1.2 m/s, the total stored energy capacity will increase from 571.80 kJ to 669.49 kJ, which increases about 17.08%. However, the increment of stored energy capacity decreases with the increasing velocity. The curve indicates that the energy storage rate increases with the increase of inlet velocity of HTF, and the inlet velocity increasing from 0.2 m/s to 1.2 m/s, the total energy storage rate will increase from 50.45 J/s to 96.02 J/s, which increases about double. It can be seen that the inlet velocity of the HTF has a great influence on the heat storage characteristics of the TES tank in the CSP system.

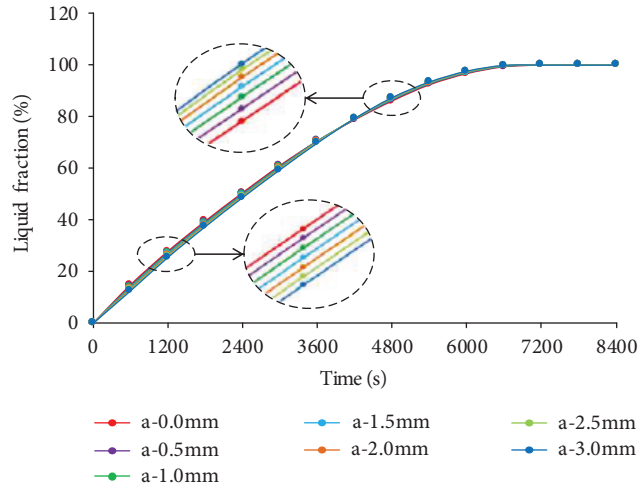

Figure 5: Effects of thickness of tube on liquid fraction.

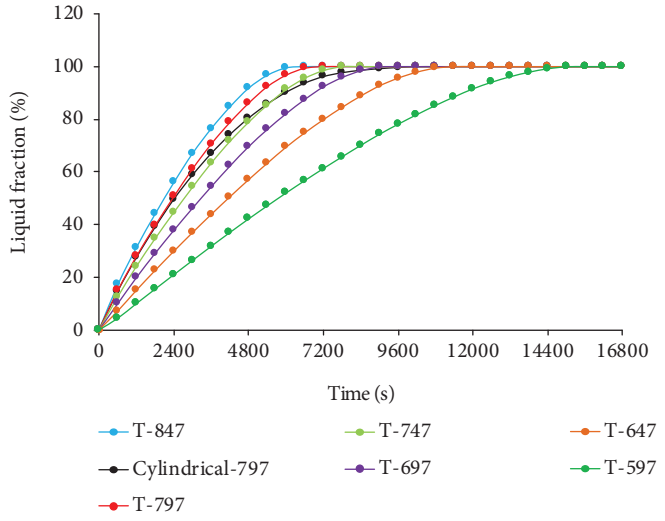

Figure 6: Effects of inlet temperature of HTF on liquid fraction.

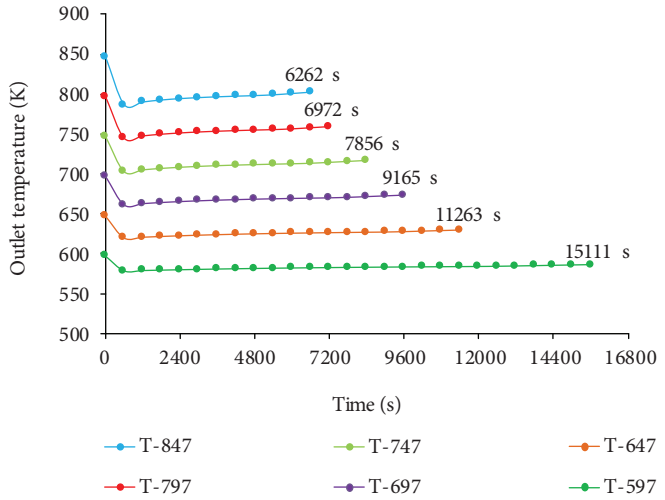

Figure 7: Effects of inlet temperature of HTF on outlet temperature of HTF.

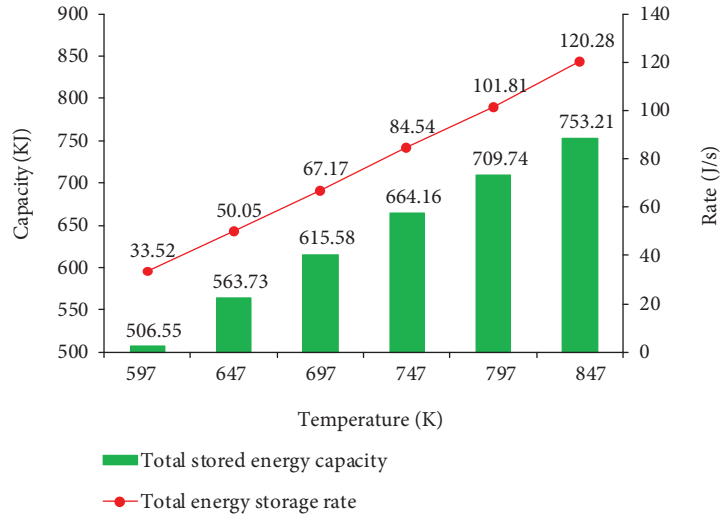

Figure 8: Effects of inlet temperature of HTF on the total stored energy capacity and energy storage rate.

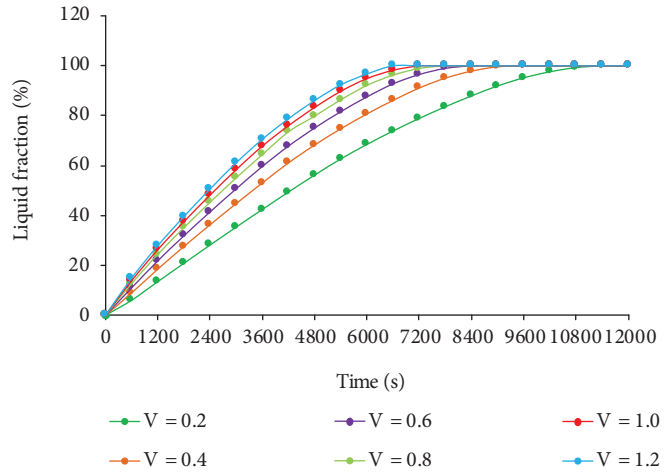

Figure 9: Effects of inlet velocity of HTF on liquid fraction.

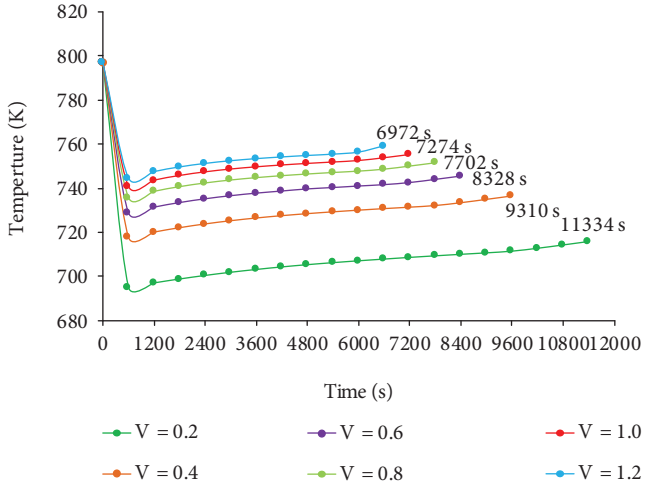

Figure 10: Effects of inlet velocity of HTF on outlet temperature of HTF.

4.2. Discharging Process of TES

4.2.1. Comparison of the TES Performance between Cylindrical and Truncated Cone TES Model during the Discharging Process. In order to compare the thermal energy release performance between traditional cylindrical and truncated cone TES tanks, the inlet temperature and velocity of HTF are 377 K and 1.2 m/s, respectively, and the initial temperature of PCM and steel is 507 K.

The contour of the PCM liquid fraction and temperature field in the cylindrical and truncated cone model during the discharging process are shown in Figure 12. It is found that the PCM begins to solidify at the surface of the heat conduction tube wall, and the upper region of PCM solidification is firstly compared to the bottom region of PCM. In this process, it can be seen that the temperature field is consistent with the solid-liquid phase of the PCM in TES tank. On the whole, the temperature of upper PCM is lower than the bottom region. This phenomenon can directly explain the reason that the upper PCM completed the solidification process firstly.

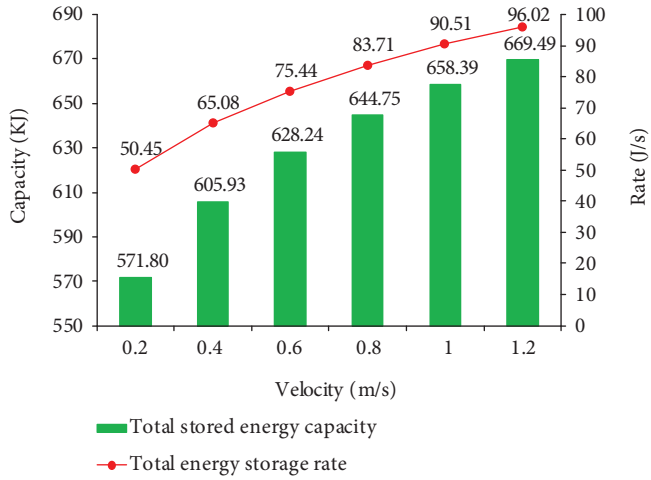

Figure 11: Effects of inlet velocity of HTF on the total stored energy capacity and energy storage rate.

From the total discharging process, the truncated cone tank can solidify slightly faster than the cylindrical tank at the same operating condition during the discharging process. The liquid fraction difference of them is only 0.64% at 3600 s, which shows the thermal energy release rate is almost parallel at the beginning. After that, the liquid fraction of a truncated cone tank is decreasing faster than a cylindrical tank. It can be found that the discharging rate of a truncated cone unit is faster than a cylindrical tank, and the discharging time reduces about 21.59% compared to the cylindrical model. This indicates that the thermal energy release performance of truncated cone TES tank is slightly better than the traditional cylindrical tank for CSP plant under the same operating condition.

And Figure 13 presents the simulated liquid PCM velocity field with truncated cone TES tank at 3600 s. It can be seen that the anticlockwise convection circulation arises at the liquid region of PCM. And the high-temperature liquid PCM at the vicinity of shell flows upward due to the effect of natural convection, which is weakened compared to the charging process. Whereas the low-temperature liquid PCM flows downward along the liquid/solid PCM interface because of the natural gravity, which is accelerated compared to the charging process. In this situation, the natural convection makes the higher-temperature liquid PCM flow upward, which accelerates the thermal energy releasing at the upper region of PCM during the discharging process due to the lower temperature at the top of HTF. Therefore, the truncated cone TES tank can also reduce the discharging time compared to the traditional cylindrical TES tank.

4.2.2. Effects of Inlet Temperature of HTF on Discharging Process. In order to investigate the effects of initial inlet temperature of HTF on discharging process, the inlet velocity of HTF is 1.2 m/s, the initial temperature of PCM is 507 K, and the inlet temperature of the HTF is six temperature gradients, including 377 K, 387 K, 397 K, 407 K, 417 K, and 427 K. The thickness of tube is neglected due to its slight effect on thermal energy storage performance.

Figure 14 shows the effects of initial inlet temperature of HTF on discharging time and liquid fraction of PCM during the discharging process, which include the discharging process of cylindrical TES tank under the inlet temperature of HTF at 377 K. It can be seen that the slope of the curves of the TES tanks decreases gradually under different inlet temperatures of HTF, which indicates that the thermal energy release rate of the TES tanks reduce gradually. The larger the inlet temperature of the HTF is, and the smaller the slope of the whole corresponding curve is. Under the same operating conditions, the total discharging time of the truncated cone TES tank is shorter than that of the cylindrical tank. The results are consistent with the contour of the PCM liquid fraction and temperature in the cylindrical and truncated cone tank during the discharging process (Figure 12).

When the inlet temperature of the HTF is 377 K, it takes 12,920 s for the cylindrical tank to complete the discharging process and only 10,130 s for the truncated cone tank, which reduces 21.59%. For the truncated cone TES tank, the discharging time increases with the increasing inlet temperature. When the inlet temperature of HTF increase from 377 K to 427 K, the discharging time will increase from 10,130 s to 15,380 s, which increases about 51.82%. It can be seen that the inlet temperature of HTF has great influence on the discharging process of the TES tank in the CSP system, and the thermal energy release performance of the truncated cone TES tank is better than the cylindrical tank.

Figure 15 presents the effects of inlet temperature of HTF on the total released energy capacity and total energy release rate during the discharging process, which include the results of cylindrical TES tank under the inlet temperature at 377 K ("C-377" in Figure 15). And the total released energy capacity is calculated by equation (5). The total energy release rate is calculated by the following equation.

$$v_{Q'} = \frac{Q'}{t}, \tag{7}$$

where the $v_{Q'}$ represents the total energy release rate

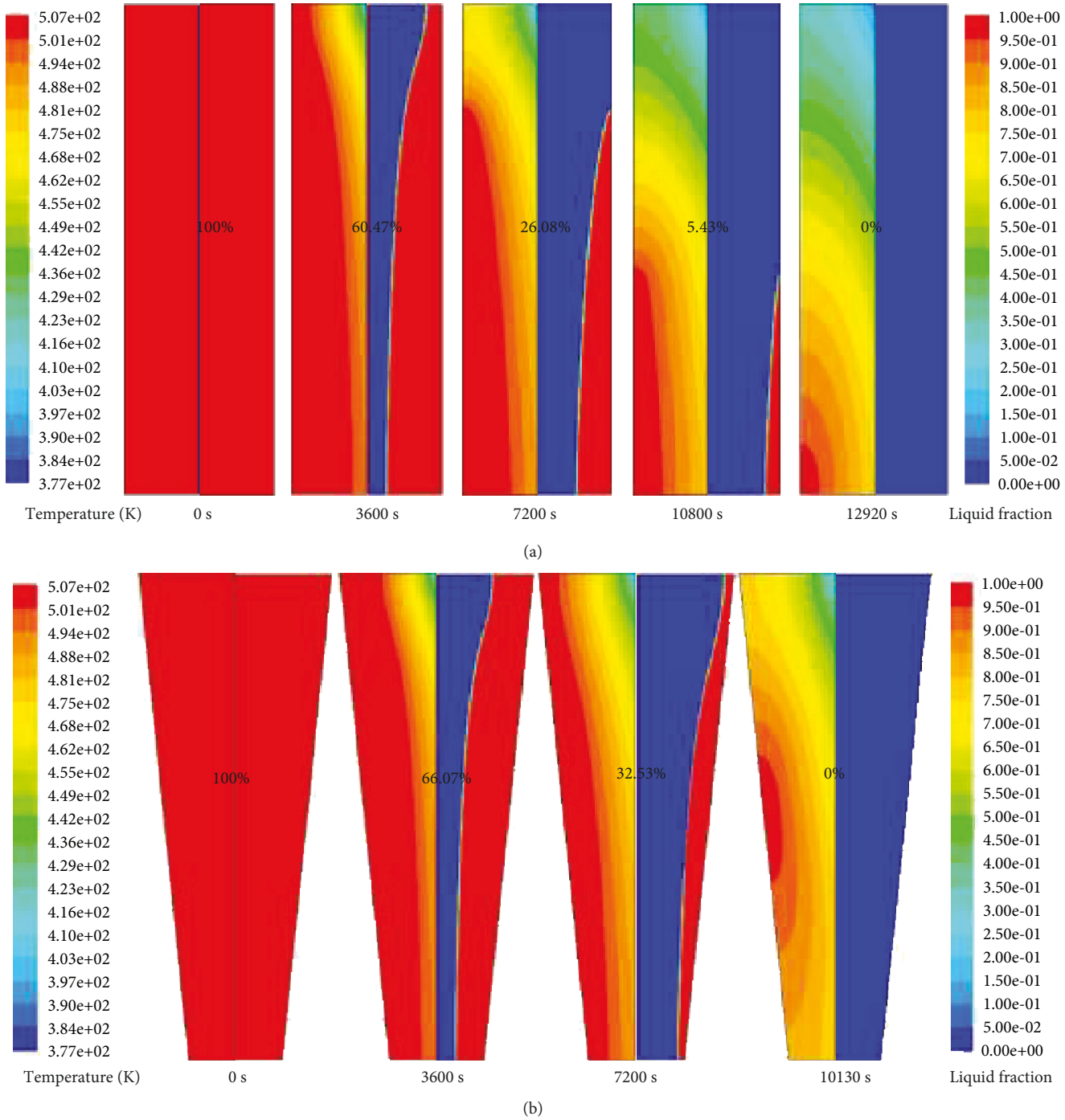

Figure 12: Contour of the PCM temperature (left) and liquid fraction (right) in the (a) cylindrical and (b) truncated cone model during the solidification process.

(J/s), Q' is the total released energy capacity (J), and t is the discharging time (s).

When the inlet temperature is 377 K, it can be seen that the total released energy capacity of the cylindrical tank (537.91 kJ) is much larger than that of the truncated cone TES tank (469.53 kJ). However, the energy release rate of the truncated cone tank is greater than that of the cylindrical tank, which increases 9.87% compared to the cylindrical tank. It can be found that the heat energy utilization rate from the PCM of the truncated cone TES tank is higher than that of the cylindrical tank.

For truncated cone TES tank, the total released energy capacity decreases with the increase of the inlet temperature of HTF in Figure 15. And the initial inlet temperature of HTF increasing from 377 K to 427 K, the total released energy capacity will decrease from 469.53 kJ to 439.06 kJ, which

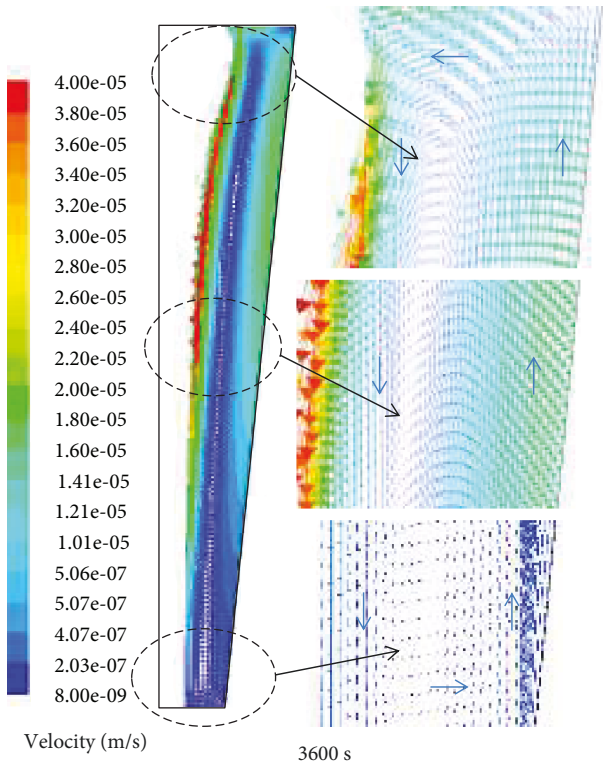

Figure 13: The simulated liquid PCM velocity field with truncated cone TES unit during discharging process.

reduces about 6.49%. Meanwhile, the curve shows that the total energy release rate decreases significantly with the increasing inlet temperature of HTF, and the initial inlet temperature increasing from 377 K to 427 K, the total energy release rate will decrease from 46.19 J/s to 28.48 J/s, which reduces about 38.34%.

4.2.3. Effects of Inlet Velocity of HTF on Discharging Process. In order to investigate the influence of inlet velocity of HTF on the discharging process of a truncated cone TES tank, according to the results of the inlet temperature for HTF on the heat discharging process, the inlet temperature of 397 K is selected to the study. The initial temperature of PCM is 507 K, and the inlet velocity of the HTF is six temperature gradients, including 0.2 m/s, 0.4 m/s, 0.6 m/s, 0.8 m/s, 1.0 m/s, and 1.2 m/s.

The effect of inlet velocity of HTF on liquid fraction and discharging process is shown in Figure 16. From the curves, the slope of curves is gradually decreasing during the discharging process. With the increase of the inlet velocity of HTF, the discharging time is gradually shortened, and the amplitude of the shortening is gradually reduced. Thus, the smaller the inlet velocity of the HTF is, the larger the effect on the discharging time of the TES tank is. The inlet velocity of HTF increasing from 0.2 m/s to 1.2 m/s, the discharging time will decrease from 19,270 s to 12,150 s, which reduces about 36.95%.

Figure 17 presents the effects of inlet velocity of HTF on the total released energy capacity and total energy release rate during the discharging process. From the histograms and curve, the total released energy capacity and energy release rate increase with the increase of inlet velocity of HTF. And inlet velocity of HTF increasing from 0.2 m/s to 1.2 m/s, the released energy capacity will increase from 440.92 kJ to 455.36 kJ, which increases slightly about 3.27%. And the total energy release rate increases about 65.17%. This is because with the increase of the inlet velocity of the HTF, the total released energy capacity increases, while the total discharging time decreases gradually, which leads to the phenomenon that the total energy release rate increases greatly.

4.3. Analysis of Heat Storage Efficiency of TES Tank. In order to analyze the heat storage efficiency of the truncated cone TES tank, firstly, the heat storage efficiency is calculated by following equation.

$$\eta = \frac{Q'}{Q}, \tag{8}$$

where the Q' and Q is the total released energy capacity and total stored energy capacity, respectively.

Then, according to the above results, the stored and released energy capacity in a truncated cone TES tank has been calculated. In this process, the influence of the inlet temperature and velocity of the HTF on the heat storage efficiency of the truncated cone TES tank can be compared and analyzed.

Figure 18 shows the influence of the inlet temperature of the HTF on the storage efficiency of the TES tank, in which the x-axis is the inlet temperature of the HTF during the charging process, the y-axis is the heat storage efficiency, and the legend shows the inlet temperature of HTF during the discharging process.

From the diagram, it can be found that the heat storage efficiency decreases with the increase of the inlet temperature of HTF in the charging process. And the maximum heat storage efficiency of the TES tank can reach 93% and the minimum is about 58%, which indicated that the inlet temperature of the HTF has a great influence on the heat storage efficiency of the TES system in CSP plant.

When the inlet temperature of the HTF is constant during the charging process, the higher the inlet temperature of the HTF during the discharging process is, the lower the heat storage efficiency of the TES tank is. Meanwhile, when the inlet temperature of the HTF is constant during the discharging process, the higher the inlet temperature of the HTF during the charging process is, the lower the heat storage efficiency of the TES tank is. Compared with the discharging process, the inlet temperature of HTF in the charging process has the more significant effect on the heat storage efficiency. As a whole, the lower the inlet temperature of the HTF is, the higher the thermal energy utilization efficiency is, that is, the higher the heat storage efficiency of the TES tank is.

The influence of the inlet velocity of the HTF on the storage efficiency of the TES tank is shown in Figure 19, in which the x-axis is the inlet velocity of the HTF during the charging process, the y-axis is the heat storage efficiency,

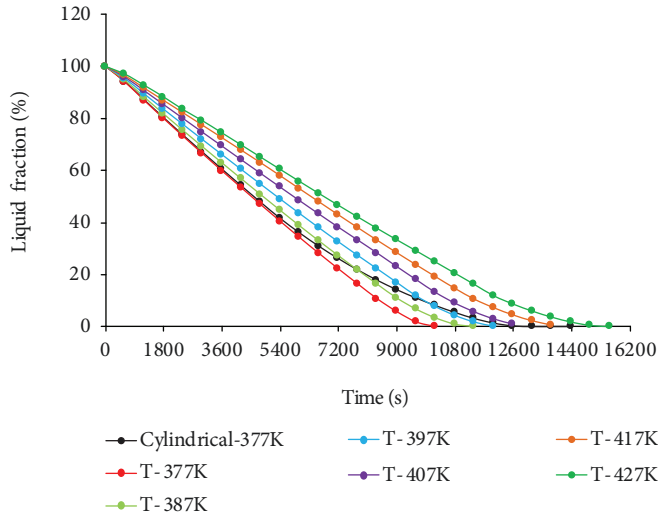

Figure 14: Effects of initial inlet temperature of HTF on liquid fraction.

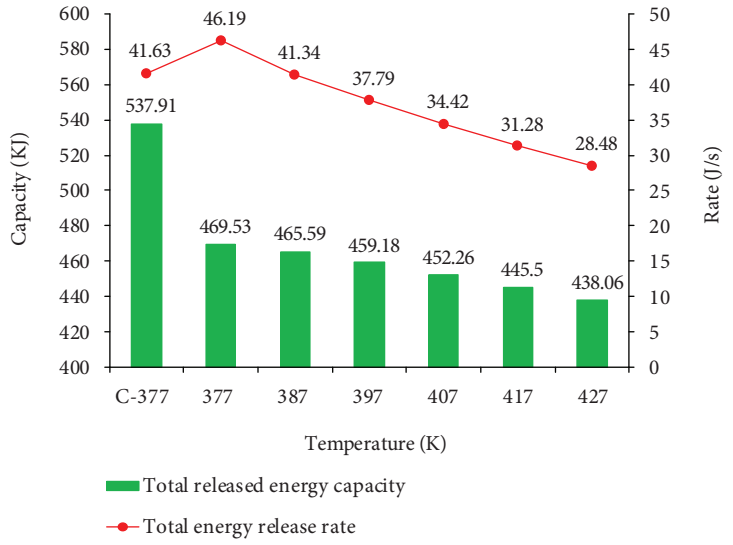

Figure 15: Effects of inlet temperature of HTF on the total released energy capacity and energy release rate.

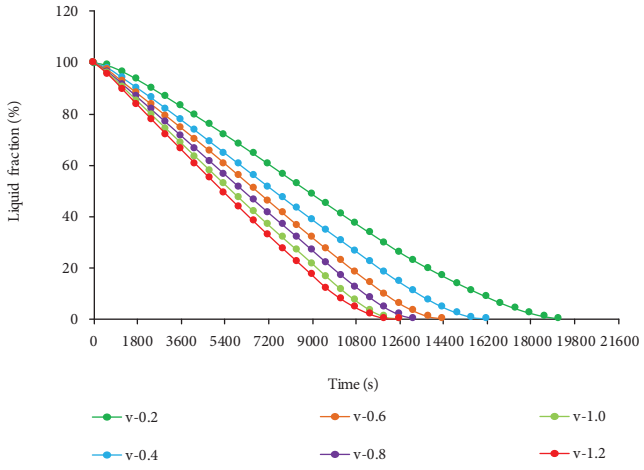

Figure 16: Effects of inlet velocity of HTF on liquid fraction.

and the legend shows the inlet velocity of HTF during the discharging process.

It can be found that the heat storage efficiency decreases with the increase of the inlet velocity of HTF in the charging process. In the calculation range, the range of heat storage efficiency of a truncated cone TES tank is 80% ~ 65%, and the effect of velocity on the heat storage efficiency of TES tank is slighter than the influence of the inlet temperature of HTF on it.

When the inlet velocity of the HTF is constant during the charging process, the higher the inlet velocity of the HTF during the discharging process is, the higher the heat storage efficiency of the heat storage tank is. However, when the inlet velocity of the HTF is constant during the discharging process, the higher the inlet velocity of the HTF during the charging process is, the lower the heat storage efficiency of the TES tank is. And compared with the discharging

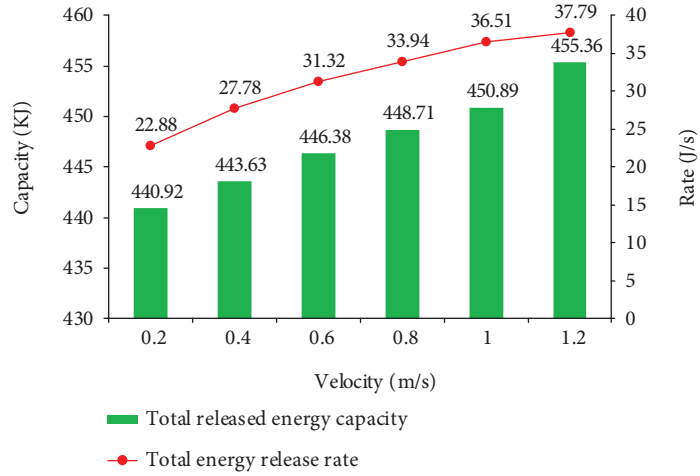

Figure 17: Effects of inlet velocity of HTF on the total released energy capacity and energy release rate.

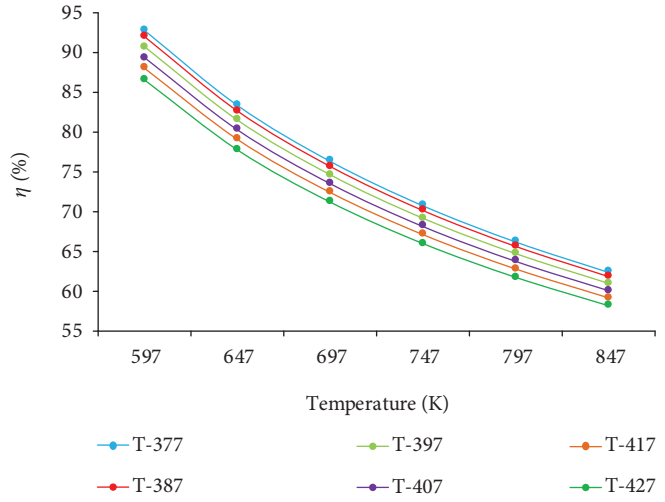

Figure 18: Effect of inlet temperature of HTF on heat storage efficiency.

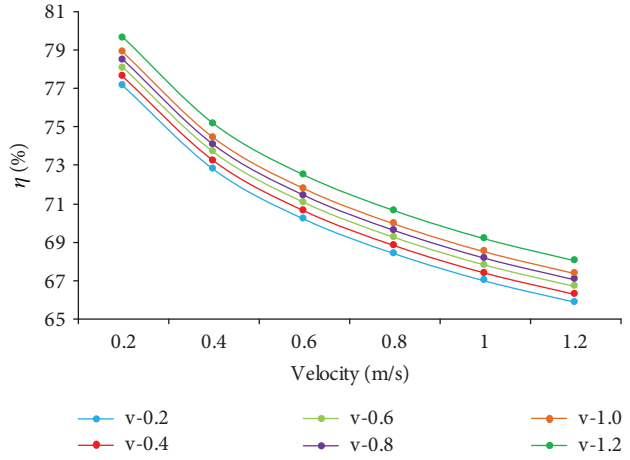

Figure 19: Effect of inlet velocity of HTF on heat storage efficiency.

process, the inlet velocity of HTF in the charging process has also the more significant effect on the heat storage efficiency. As a whole, the lower the inlet velocity of the HTF is during the charging process and the higher the inlet velocity of HTF is during the discharging process, the higher the thermal energy utilization efficiency is, that is, the higher the heat storage efficiency of the TES tank is in the CSP system. It can be concluded that the inlet condition (temperature and velocity) of HTF in the charging process has the more obvious impact on the heat storage efficiency of TES system in CSP technology.

5. Conclusions

Developing CSP technology is one of the most effective ways to solve energy shortage all over the world. And the TES system is the key to improve the performance of CSP system. In this paper, a two dimensional physical and mathematical model for a novel truncated cone shell-and-tube TES tank has been established based on enthalpy method. Then, the

charging/discharging process of the cylindrical tank and the novel tank has been compared. Meanwhile, the effects of inlet conditions of HTF, and thickness of tube on the charging/discharging process, and heat storage efficiency have been investigated. The following conclusions can be drawn.

(1) Comparing the performance between cylindrical and truncated cone TES tank, it can be seen that the performance of truncated cone tank is better under the same operating condition, which reduces the charging/discharging time about 32.08% and 21.59%, respectively. And the velocity field of liquid PCM during the charging/discharging process shows clockwise/anticlockwise convection circulation

(2) The effect of thickness of tube on the charging process of PCM is slight, so the effect of wall thickness on the TES system can be ignored

(3) During the charging process, with the increase of the inlet temperature of HTF, the charging time reduces about 58.56%, and the stored energy capacity and energy storage rate increase about 48.69% and four times. With the increasing inlet velocity, the melting time reduces about 38.48%, and the stored energy capacity and energy storage rate increase about 17.08% and double. However, the thermal energy utilization rate of HTF is very low

(4) During the discharging process, with the increase of inlet temperature of HTF, the discharging time increases 51.82%, and the released energy capacity and energy release rate reduce about 6.49% and 38.34%, respectively. With the increasing velocity, the discharging time reduces about 36.95%, and the released energy capacity and energy release rate will increase about 3.27% and 65.17%, respectively

(5) For the heat storage efficiency, the maximum heat storage efficiency of the truncated cone TES tank can reach 93% in the range of the simulation

(6) Therefore, the initial operating condition of HTF is the significant factor in the practical applications of the CSP system. Particularly, some appropriate methods should be studied for reducing the loss of energy and improving the thermal energy utilization rate of HTF in the next study. And this researcher will provide the significant reference towards geometric design and operating conditions by considering the effect of natural convection on the TES system in the CSP plants

Nomenclature

C_p: Specific heat, J/(kg·K)
f: Liquid fraction
h: Heat transfer coefficient, W/m^2·K
v: Velocity, m/s
v_{max}: The maximum velocity, m/s
P_r: Prandtl number
R_e: Reynolds number
Re_{max}: The maximum Reynolds number
Q: Total stored energy capacity, J
Q': Total released energy capacity, J
t: Charging/discharging time, s
v_Q: Total energy storage rate, J/s
$v_{Q'}$: Total energy release rate, J/s
m: The mass of the PCM, kg
R_{in}: The radius of the inner tube, mm
R: The radius of the shell side or the top of the truncated cone model, mm
r: The radius of the bottom of the truncated cone model, mm
a: The thickness of the tube, mm
L: The length of the PCM unit, mm
T: Temperature, K
T_m: Melting point temperature of PCM, K
T_a: The average temperature of PCM, K
T_0: The initial temperature, K
CSP: Concentrated solar power
PCM: Phase change material
TES: Thermal energy storage
HTF: Heat transfer fluid
LHTES: Latent heat thermal energy storage

Greek Symbols

ρ: Density, kg/m^3
λ: Thermal conductivity, W/m·K
λ_p: Thermal conductivity of PCM in r direction, W/m·K
λ'_p: Thermal conductivity of PCM in x direction, W/m·K
ΔH: Enthalpy, kJ/kg
η: Heat storage efficiency

Data Availability

The data used to support the findings of this study are available from the corresponding author upon request.

Conflicts of Interest

The authors declare that there is no conflict of interests regarding the publication of this paper.

Acknowledgments

This work is supported by the National Natural Science Foundation of China (Nos. 51876147 and 51406033). Besides, a very special acknowledgement is made to the editors and referees who made important comments to improve this paper.

References

[1] Z. D. Cheng, Y. L. He, F. Q. Cui, R. J. Xu, and Y. B. Tao, "Numerical simulation of a parabolic trough solar collector with nonuniform solar flux conditions by coupling FVM and MCRT method," *Solar Energy*, vol. 86, no. 6, pp. 1770–1784, 2012.

[2] B. Xu, P. Li, and C. Chan, "Application of phase change materials for thermal energy storage in concentrated solar thermal power plants: a review to recent developments," *Applied Energy*, vol. 160, pp. 286–307, 2015.

[3] Q. Mao, "Recent developments in geometrical configurations of thermal energy storage for concentrating solar power plant," *Renewable and Sustainable Energy Reviews*, vol. 59, pp. 320–327, 2016.

[4] S. Kuravi, J. Trahan, D. Y. Goswami, M. M. Rahman, and E. K. Stefanakos, "Thermal energy storage technologies and systems for concentrating solar power plants," *Progress in Energy and Combustion Science*, vol. 39, no. 4, pp. 285–319, 2013.

[5] G. Alva, L. Liu, X. Huang, and G. Fang, "Thermal energy storage materials and systems for solar energy applications," *Renewable and Sustainable Energy Reviews*, vol. 68, pp. 693–706, 2017.

[6] A. K. Pandey, M. S. Hossain, V. V. Tyagi, N. Abd Rahim, J. A. L. Selvaraj, and A. Sari, "Novel approaches and recent developments on potential applications of phase change materials in solar energy," *Renewable and Sustainable Energy Reviews*, vol. 82, pp. 281–323, 2018.

[7] H. J. Xu and C. Y. Zhao, "Thermal performance of cascaded thermal storage with phase-change materials (PCMs). Part I: steady cases," *International Journal of Heat and Mass Transfer*, vol. 106, pp. 932–944, 2017.

[8] Y. Q. Li, Y. L. He, H. J. Song, C. Xu, and W. W. Wang, "Numerical analysis and parameters optimization of shell-and-tube heat storage unit using three phase change materials," *Renewable Energy*, vol. 59, pp. 92–99, 2013.

[9] G. Wei, G. Wang, C. Xu et al., "Selection principles and thermophysical properties of high temperature phase change materials for thermal energy storage: a review," *Renewable and Sustainable Energy Reviews*, vol. 81, pp. 1771–1786, 2018.

[10] M. Avci and M. Y. Yazici, "Experimental study of thermal energy storage characteristics of a paraffin in a horizontal tube-in-shell storage unit," *Energy Conversion and Management*, vol. 73, pp. 271–277, 2013.

[11] M. Dadollahi and M. Mehrpooya, "Modeling and investigation of high temperature phase change materials (PCM) in different storage tank configurations," *Journal of Cleaner Production*, vol. 161, pp. 831–839, 2017.

[12] Y. B. Tao and Y. L. He, "Numerical study on thermal energy storage performance of phase change material under non-steady-state inlet boundary," *Applied Energy*, vol. 88, no. 11, pp. 4172–4179, 2011.

[13] Y. Fang, J. Niu, and S. Deng, "Numerical analysis for maximizing effective energy storage capacity of thermal energy storage systems by enhancing heat transfer in PCM," *Energy and Buildings*, vol. 160, pp. 10–18, 2018.

[14] M. R. Assari, H. Basirat Tabrizi, and M. Savadkohy, "Numerical and experimental study of inlet-outlet locations effect in horizontal storage tank of solar water heater," *Sustainable Energy Technologies and Assessments*, vol. 25, pp. 181–190, 2018.

[15] S. Seddegh, M. M. Joybari, X. Wang, and F. Haghighat, "Experimental and numerical characterization of natural convection in a vertical shell-and-tube latent thermal energy storage system," *Sustainable Cities and Society*, vol. 35, pp. 13–24, 2017.

[16] Y. B. Tao and Y. L. He, "Effects of natural convection on latent heat storage performance of salt in a horizontal concentric tube," *Applied Energy*, vol. 143, pp. 38–46, 2015.

[17] J. C. Kurnia and A. P. Sasmito, "Numerical investigation of heat transfer performance of a rotating latent heat thermal energy storage," *Applied Energy*, vol. 227, pp. 542–554, 2018.

[18] X. Gao, P. Wei, Y. Xie et al., "Experimental investigation of the cubic thermal energy storage unit with coil tubes," *Energy Procedia*, vol. 142, pp. 3709–3714, 2017.

[19] M. Parsazadeh and X. Duan, "Numerical study on the effects of fins and nanoparticles in a shell and tube phase change thermal energy storage unit," *Applied Energy*, vol. 216, pp. 142–156, 2018.

[20] X. Yang, Z. Lu, Q. Bai, Q. Zhang, L. Jin, and J. Yan, "Thermal performance of a shell-and-tube latent heat thermal energy storage unit: role of annular fins," *Applied Energy*, vol. 202, pp. 558–570, 2017.

[21] M. E. H. Amagour, A. Rachek, M. Bennajah, and M. Ebn Touhami, "Experimental investigation and comparative performance analysis of a compact finned-tube heat exchanger uniformly filled with a phase change material for thermal energy storage," *Energy Conversion and Management*, vol. 165, pp. 137–151, 2018.

[22] J. Gasia, J. Diriken, M. Bourke, J. van Bael, and L. F. Cabeza, "Comparative study of the thermal performance of four different shell-and-tube heat exchangers used as latent heat thermal energy storage systems," *Renewable Energy*, vol. 114, pp. 934–944, 2017.

[23] F. Zhu, C. Zhang, and X. Gong, "Numerical analysis and comparison of the thermal performance enhancement methods for metal foam/phase change material composite," *Applied Thermal Engineering*, vol. 109, pp. 373–383, 2016.

[24] M. Eslami and M. A. Bahrami, "Sensible and latent thermal energy storage with constructal fins," *International Journal of Hydrogen Energy*, vol. 42, no. 28, pp. 17681–17691, 2017.

[25] M. Parsazadeh and X. Duan, "Numerical and statistical study on melting of nanoparticle enhanced phase change material in a shell-and-tube thermal energy storage system," *Applied Thermal Engineering*, vol. 111, pp. 950–960, 2017.

[26] S. Bellan, T. E. Alam, J. González-Aguilar et al., "Numerical and experimental studies on heat transfer characteristics of thermal energy storage system packed with molten salt PCM capsules," *Applied Thermal Engineering*, vol. 90, pp. 970–979, 2015.

[27] F. Ma and P. Zhang, "Investigation on the performance of a high-temperature packed bed latent heat thermal energy storage system using Al-Si alloy," *Energy Conversion and Management*, vol. 150, pp. 500–514, 2017.

[28] A. Abdulla and K. S. Reddy, "Effect of operating parameters on thermal performance of molten salt packed-bed thermocline thermal energy storage system for concentrating solar power plants," *International Journal of Thermal Sciences*, vol. 121, pp. 30–44, 2017.

[29] M. A. Kibria, M. R. Anisur, M. H. Mahfuz, R. Saidur, and I. H. S. C. Metselaar, "Numerical and experimental investigation of heat transfer in a shell and tube thermal energy storage system," *International Communications in Heat and Mass Transfer*, vol. 53, pp. 71–78, 2014.

[30] Y. B. Tao and Y. L. He, "Numerical study on performance enhancement of shell-and-tube latent heat storage unit,"

International Communications in Heat and Mass Transfer, vol. 67, pp. 147–152, 2015.

[31] K. S. Reddy, V. Mudgal, and T. K. Mallick, "Review of latent heat thermal energy storage for improved material stability and effective load management," *Journal of Energy Storage*, vol. 15, pp. 205–227, 2018.

[32] Q. Mao, H. Chen, Y. Zhao, and H. Wu, "A novel heat transfer model of a phase change material using in solar power plant," *Applied Thermal Engineering*, vol. 129, pp. 557–563, 2018.